

Diffusion-Weighted and Dynamic Contrast-Enhanced MRI to Assess Radiation Therapy Response for Head and Neck Paragangliomas

**Authors:** Yoshiaki Ota, Eric Liao, Ryo Kurokawa, Faiz Syed, Akira Baba, Mariko Kurokawa, Toshio Moritani, Ashok Srinivasan

**Department and Institution:** The Division of Neuroradiology, Department of Radiology, University of Michigan, 1500 E Medical Center Dr, UH B2, Ann Arbor, MI 48109, USA

**Running title:** DWI and DCE-MRI for RT response in paragangliomas

**Keywords:** DWI; DCE-MRI; paraganglioma; radiation therapy; head and neck

**Corresponding author:** Yoshiaki Ota

Address: 1500 E Medical Center Dr, UH B2, Ann Arbor, MI 48109, USA

Phone: 7348825904

FAX number: 7346159800

Email address: yoshiako@med.umich.edu

**Acknowledgements and Disclosure:** There is no fund or grant support for this study. The authors declare that they have no competing interests.

This is the author manuscript accepted for publication and has undergone full peer review but has not been through the copyediting, typesetting, pagination and proofreading process, which may lead to differences between this version and the [Version of Record](#). Please cite this article as [doi: 10.1111/jon.12875](https://doi.org/10.1111/jon.12875).

This article is protected by copyright. All rights reserved.

## Abstract

**Background and Purpose:** The prediction of radiotherapy outcome in head and neck paragangliomas is clinically important. We investigated perfusion and diffusion markers for evaluation of response to radiotherapy of head and neck paragangliomas.

**Methods:** We retrospectively reviewed 330 consecutive patients from January 2016 to September 2019 with suspected head and neck paragangliomas, and enrolled 11 patients (2 male, 9 female; age:  $55.2 \pm 10.3$  years) who had conventional MRI and dynamic contrast-enhanced (DCE)-MRI before and after radiation therapy. Radiation therapy, consisting of external beam radiotherapy or stereotactic radiotherapy, was conducted at the radiation oncology department in a single center. Mean apparent diffusion coefficient (ADC), normalized mean ADC, and parameters of DCE-MRI were compared between pre- and post-treatment status by paired t-test. The Pearson correlation coefficient was used for the relationship between tumor volume ratio (post-treatment status/pre-treatment status) and pre-treatment and post-treatment values.

**Results:** Mean and normalized ADC values were statistically higher in post-treatment status than pre-treatment status ( $P=.005$ ,  $P=.005$ , respectively), and  $K_{trans}$  (volume transfer constant between extravascular, extracellular space (EES) and blood plasma per minute) and  $K_{ep}$  (rate transfer constant between EES and blood plasma per minute) were significantly lower in post-treatment status than pre-treatment status ( $P=.007$ ,  $P=.027$ , respectively). The correlation coefficient of the

relationship between tumor volume ratio and pre-treatment Ktrans ( $r=0.70$ ;  $P= .016$ ) and between tumor volume ratio and post-treatment Ktrans and Kep ( $r=0.83$ ;  $P= .002$ ,  $r=0.8$ ;  $P=.003$ , respectively) was statistically significant.

**Conclusions:** Ktrans has predictive potential to predict the response to radiation therapy of head and neck paragangliomas.

## Introduction

Paragangliomas are uncommon neuroendocrine tumors arising from the sympathetic and parasympathetic autonomic system and occur anywhere from the base of the skull to the pelvis. 70% of extra-adrenal paragangliomas arise in the head and neck region, with an estimated annual incidence of 3–8 cases per 1 million people in general population.<sup>1</sup> The typical clinical sites of head and neck paragangliomas are the carotid artery bifurcation, the middle ear, and jugular fossa.<sup>1–3</sup> On conventional MRI, paragangliomas usually show hypointensity on T1-weighted images, isointensity to hyperintensity on T2-weighted images, and intense heterogeneous enhancement on contrast-enhanced T1-weighted images. Signal voids related to the high flow within the tumor are common with a “salt-and-pepper appearance”.<sup>4</sup> In carotid bifurcation lesions, splaying of the carotid bifurcation has been described on MRI and computed tomography (CT) angiography.<sup>4</sup> Treatment options for paragangliomas include surgery and radiation therapy (RT), which depends on the

location, the size of the tumor, the patient's age and condition, or the anticipated morbidity of the treatment alternatives.<sup>5</sup>

Typically, RT is chosen to treat when the patients is elderly, or when the tumor is deemed unresectable. The goal of RT is to halt further tumor progression. Generally, the size of the treated residual mass is stable or gradually regresses, and it is extremely rare for the mass to completely disappear.<sup>5</sup> As long as the tumor does not progress, treatment goals have been met. In fact, the cumulative rate of local size control is approximately 90%,<sup>6</sup> with rare cases of progression after RT.

Radiation-associated imaging changes on MRI include decrease of flow voids within the tumor, decreased heterogeneous enhancement and reduced T2 signal of tumor.<sup>7</sup> However, there have not been any established parameters for detection of the response to RT in head and neck paragangliomas. Recently, magnetic resonance techniques such as diffusion-weighted imaging (DWI)<sup>8</sup> and dynamic contrast-enhanced (DCE)-MRI<sup>9,10</sup> have been proposed as such noninvasive imaging parameters for prediction and early detection of response to cancer therapy for various organs. Diffusion-weighted images (DWI) can be used for diagnosis, staging, and follow-up of head and neck tumors<sup>11</sup> based on the fact that apparent diffusion coefficient (ADC) value can reflect the solid tumor's cellularity. DCE-MRI demonstrates functional characteristics of the tumor such as vascularity and permeability. Therefore, DWI and DCE-MRI can allow for evaluation of the RT response.

This study investigated these values for prediction of RT response in head and neck paragangliomas.

## Methods

Our institutional review board approved this retrospective single-center study and waived the requirement for informed consent. Data was acquired in compliance with all applicable Health Insurance Portability and Accountability Act regulations.

### *Study population*

We retrospectively reviewed the medical records of 330 consecutive patients from January 2016 to September 2019 who were suspected of head and neck paragangliomas. There were 94 patients who were diagnosed with paragangliomas histopathologically, or clinically diagnosed by elevated plasma fractionated metanephrines or elevated 24-hour urinary fractionated metanephrines, imaging findings of head and neck conventional CT and MRI, and positron emission tomography with 2-deoxy-2-[fluorine-18] fluoro-D-glucose integrated with CT or <sup>111</sup>In-pentetreotide single-photon emission CT. We excluded patients who had been previously treated with operation or embolization, or did not have pretreatment or posttreatment DWI and DCE-MRI.

Eleven patients (2 male, 9 female; age  $55.2 \pm 10.3$  years; age range 36–69 years) who had pre- and post-treatment DWI and DCE-MRI were included in this study. 4 patients were pathologically

This article is protected by copyright. All rights reserved.

proven, and 7 patients were clinically diagnosed. Post-treatment conventional MRI and DCE-MRI were performed 12 months after radiation therapy. After radiation therapy, any direct procedures or interventions such as biopsies or any additional treatments such as surgery, chemotherapy, or embolization were not performed.

### *Radiation therapy*

All patients had conventional external beam radiation therapy (EBRT) or stereotactic radiotherapy at the radiation oncology department in our institution.

The dose of 45 or 50 gray for 25 fractions of EBRT was delivered to 8 patients. The dose of 25 or 30 gray for 5 fractions of stereotactic radiotherapy was delivered to 3 patients.

### *MRI acquisition*

MRI examinations were performed using 1.5T and 3T (Ingenia; Philips, Eindhoven) with a head and neck array coil in supine position. Pre and post T1-weighted images and DWI were used in this study.

The parameters of pre- and post T1-weighted images were as follows: plane = axial and coronal, Repetition Time (TR) = 500–800 ms, Echo Time (TE) = 5–16 ms, NEX = 1 or 2, slice thickness/gap = 3.5–5/1–1.2 mm, field of view = 180–240 mm, Matrix = 188–320 × 188–320. DWI used echo-planar imaging. Sensitizing diffusion gradients were applied sequentially with b values set at 0 and 1000

s/mm<sup>2</sup>. The parameters of DWI were as follows; plane = axial, TR = 5000–10000 ms, TE = 58–106

ms, NEX = 1 or 2, Slice thickness/gap = 3.5–4/0–1mm, field of view = 220–260 mm, Matrix =

128–200 × 128–200, Diffusion directions = 3. DCE–MRI sequence was performed using

3-dimensional T1-weighted images of 3D–T1 Fast Field Echo (FFE), with the administration of

contrast gadobenate dimeglumine (Multihance, Bracco diagnostics, Singen, Germany). An

intravenous bolus of 20 ml of gadobenate dimeglumine was administered using a power injector with a

flow rate of 5.0 mL/s through a peripheral arm vein, followed by a 20 mL saline flush. DCE–MRI was

sequentially obtained for 30 dynamic phases for each investigation. These techniques were

performed on all image systems in a single center. The parameters of 3D–T1 FFE were as follows:

TR=4.6 ms, TE= 1.86 ms, flip angle=30° , slice thickness = 5.0 mm; field of view=240 × 240 mm<sup>2</sup>,

voxel size= 1.0 × 1.0 × 5.0 mm<sup>3</sup>, NSA = 1, number of slices per dynamic scan = 48 slices, temporal

resolution = 8.4 seconds, and total acquisition time of 4 mins and 13 seconds, using 16-channel

NeuroVascular coil.

### *Data analysis*

### *Patients' demographics*

The patient's demographics were reviewed from electrical medical records, and included the

following information: age, sex, the location of the tumor, details of radiation therapy, pre-treatment

tumor size, volume ratio of the tumors between pre- and post-treatment.

### *Imaging analysis*

One board certified neuroradiologist with 7 years of experience performed the imaging analysis. The size of tumor was evaluated on axial and coronal pre- and post- T1-weighted images. The axial images where maximal size of the tumor was depicted were used for measuring the largest dimension of anteroposterior (A) and mediolateral axis (B). The coronal images were used for the longest cranio-caudal axis length (C) of the tumor. The tumor volume was calculated by  $\frac{4}{3} \pi \times \frac{1}{2} A \times \frac{1}{2} B \times \frac{1}{2} C$ .

### *ADC analysis*

ADC maps were constructed by a mono-exponential fitting model using available software (OleaSphere, Version 3.0; Olea Medical, La Ciotat, France). The 7-year-experienced radiologist carefully outlined each tumor of pre- and post-treatment status on axial post contrast T1-weighted images and transposed the freehand region of interest (ROI) to the ADC map. The ROIs were depicted on predominantly solid enhancing portions of tumors without cystic or necrotic areas on post-contrast T1-weighted images. Manually, the ROI spared the peripheral 2 mm of lesions to avoid volume averaging.<sup>12</sup> When geometric distortion was observed, the location and size were adjusted on ADC map in order for the ROI to be included within the tumor. An additional ROI was placed in the cervical spinal cord of the level of C2-C3 disc space as an internal standard, which was



included in the field of view of every study.<sup>13</sup> A normalized ADC ratio was calculated by dividing each mean ADC value of the lesion by the mean ADC value of the cervical cord in order to adjust for variation of ADC values among MRI scanners, magnetic field strengths and matrix sizes.

### *Quantitative DCE analysis*

All quantitative analyses in DCE-MRI were performed using OleaSphere 3.0 software permeability module which is based on the extended Tofts model, by which pixel-based parameter maps are calculated from time intensity curves. The same radiologist depicted the ROI on each lesion of pre- and post-treatment status on the permeability maps which predominantly showed enhancing components of tumors. The same radiologist placed an ROI on the external carotid artery of the affected side as arterial input function. The calculated quantitative parameters were Vp (blood plasma volume per unit tissue volume), Ve (extravascular, extracellular space (EES) volume per unit tissue volume), Kep (rate transfer constant between EES and blood plasma per minute) and Ktrans (volume transfer constant between EES and blood plasma per minute).

### *Statistical analysis*

The mean ADC, normalized mean ADC values, Vp, Ve, Kep, and Ktrans were compared between pre-treatment status and post-treatment status by paired sample-test.

The Pearson correlation coefficient was used for the relationship between ratio of volume (post-treatment/pre-treatment status) and pre-treatment and post-treatment parameters. All

statistical calculations were conducted with the statistical computing language R (version 4.0.4; R Foundation for Statistical Computing, Vienna, Austria). Variables with a  $P < 0.05$  were considered as statistically significant.

## Result

### *Patients' demographics*

The patients' demographics, ADC values, and pre- and post-treatment perfusion values were summarized in Table 1. The patients were  $55.2 \pm 10.3$  years (male: 2, female: 9). 9 lesions were located in the jugular fossa (right: 3, left: 6) and 2 lesions were located at the right carotid artery bifurcation. The median pre-treatment volume of the lesion was  $13.52 \text{ cm}^3$  (range: 3.78 to  $171.1 \text{ cm}^3$ ). The median volume change ratio (post-treatment status/pre-treatment status) was 0.80 (range: 0.47 to 1.53). Representative cases of size-controlled group and size-uncontrolled group were shown in Fig 1 and Fig 2, respectively.

### *ADC values and quantitative DCE-MRI parameters analysis for pre- and post-treatment status*

Pre- and post-treatment parameters were summarized in table 2. Mean and normalized mean ADC values were significantly higher in post-treatment status than pre-treatment status (mean ADC:  $1.25 \pm 0.25$  vs  $1.36 \pm 0.20 \times 10^{-3} \text{ mm}^2/\text{s}$ ;  $P=.005$ , normalized mean ADC:  $1.50 \pm 0.33$  vs  $1.81 \pm$

0.26; P=.005, respectively). The mean ADC value of the cervical cord as an internal standard was  $0.77 \pm 0.05 \times 10^{-3}$  mm<sup>2</sup>/s. As for quantitative parameters, arterial input function curves showed a pulsed input pattern in all examination. Ktrans and Kep were significantly lower in post-treatment status than in pre-treatment status (Ktrans (minute<sup>-1</sup>):  $1.32 \pm 0.64$  vs  $0.73 \pm 0.89$ ; P=.007, Kep (minute<sup>-1</sup>):  $4.82 \pm 4.31$  vs  $2.34 \pm 2.18$ ; P=.027, respectively). Vp and Ve were not significantly different between pre- and post- treatment status. Representative cases of size-controlled group and size-uncontrolled group were shown in Fig 1 and Fig 2, respectively.

*Relationship between tumor volume ratio (post-treatment status/pre-treatment status) and pre-treatment and post-treatment parameters*

The tumor volume ratio (post-treatment status/pre-treatment status) and pre-treatment parameters were summarized in table 3. The correlation coefficient of Ktrans was statistically significant (r=0.70; P= .016) (Fig 3). The relationship between the volume ratio and other pretreatment parameters were not shown to be significantly different.

The tumor volume ratio (post-treatment status/pre-treatment status) and post-treatment parameters were summarized in table 4. The correlation coefficient of Ktrans and Kep was statistically significant (r=0.83; P= .002, r=0.8; P=.003, respectively) (Fig 3). The relationship between the volume ratio and other posttreatment parameters were not shown to be significantly different.

## Discussion

This study was designed to explore diffusion and perfusion values for detection of the response to RT of head and neck paragangliomas. In our study, mean and normalized mean ADC values were significantly higher in post-treatment status than in pre-treatment status.  $K_{trans}$  and  $K_{ep}$  were significantly lower in post-treatment status than in pre-treatment group. The tumor volume ratio and pre-treatment  $K_{trans}$ , and the tumor volume ratio and post-treatment  $K_{trans}$  and  $K_{ep}$  were correlated with significant difference. Our result implies that paragangliomas with higher  $K_{trans}$  tend to grow after the RT, and  $K_{trans}$  can be a surrogate to predict tumor response to RT. ADC values showed significant difference between pre- and post-treatment status, but the pre- and post-treatment ADC values did not show a relationship with tumor volume ratio.

DCE-MRI enables non-invasive evaluation of the tumor microvascular environment with quantitative analysis of the permeability parameters. It has been proposed that  $K_{trans}$  and  $K_{ep}$  can reflect the microvascular permeability of the tumor.<sup>14,15</sup> Paragangliomas can show different tumor cell morphology, cellularity and various histological patterns such as nests of tumor cells separated by peripheral capillaries (zellballen pattern), or large and irregular cell nest pattern.<sup>16,17</sup> Therefore, the parameters related to permeability may vary depending on the various pathologic backgrounds. For example, when paragangliomas demonstrate zellballen pattern accompanied by peripheral capillaries, which function as arteriovenous shunt, gadolinium contrast does not leak into EES, which result in

low permeability. Given our result of relationship between the tumor's volume and pre-treatment K<sub>trans</sub>, and pathologic backgrounds of head and neck paragangliomas, it is indicated that the paragangliomas with the pathological features which show high permeability even after RT leads to tumor growth. Moreover, our result suggested that the tumors with large residual size did not necessarily show higher perfusion parameters, which may imply that the residual size tumor volume does not affect the perfusion parameters.

We evaluated the ADC values on a single axial slice instead of the entire tumor volume because prior studies using volumetric ADC analyses showed no better ability than single axial section evaluations.<sup>18,19</sup> Additionally, we also performed normalized ADC values to those of the cervical spinal cord to minimize variations due to magnetic field differences. Given our strategy for standardization, we believe that our results can be validated and robust. Based on our result, ADC values significantly increased between pre- and post-treatment status without clear relationship with the tumor's volume. Increase of ADC values may represent decrease of cellularity due to RT-related change. A previous study for head and neck malignant tumor showed that ADC can be used as an effective parameter for prediction and early detection of response to RT.<sup>8</sup> According to our study, it may be postulated that paragangliomas with high permeability can grow even though cellularity is reduced after RT. As for paragangliomas, permeability parameters of DCE-MRI can be a more reliable noninvasive marker to predict response to RT than ADC values. In our study, the statistical analysis for cut-off value analysis of prediction of the outcome of RT such as tumor

regression or tumor growth was not performed due to a small cohort. The research about the prediction value is clinically important and expected to be performed with larger study population in the future.

As for tumor volume approximation, we applied three perpendicular dimensions based on the assumption that the tumor is an ellipsoid shape, as previous studies performed.<sup>20,21,22</sup> This approximation is easy to apply in clinical practice because of its simplicity. Therefore, this volume approximation seems to be a standard in the case of head and neck paragangliomas, which are ellipsoid shaped in most cases.

This study has several limitations. First, this was a retrospective study with a small cohort of patients from a single institution. Second, statistical analysis using cases with histological confirmation cannot be performed due to the small number of cases. We also included the patients which were not evaluated histopathologically, but were diagnosed based on accepted and established diagnostic tests such as elevated plasma or urinary fractionated metanephrines, imaging findings of head and neck CT and MRI, positron emission tomography with 2-deoxy-2-[fluorine-18] fluoro-D-glucose integrated with CT and <sup>111</sup>In-pentetreotide single-photon emission CT.<sup>1,4,23,24</sup> Third, DCE-MRI was performed using both 1.5T and 3T scanners.

In conclusion, Ktrans has a predictive potential to predict the response to radiation therapy of head and neck paragangliomas in this pilot study.

## Reference

1. Withey SJ, Perrio S, Christodoulou D, et al. Imaging features of succinate dehydrogenase-deficient pheochromocytoma-paranglioma syndromes. *Radiographics* 2019;39:1393-410.
2. Williams MD, Rich TA. Parangliomas arising in the head and neck: a morphologic review and genetic update. *Surg Pathol Clin* 2014;7:543-57.
3. Patel D, Phay JE, Yen TWF, et al. Update on pheochromocytoma and paranglioma from the SSO endocrine/head and neck disease-site work group. part 1 of 2: advances in pathogenesis and diagnosis of pheochromocytoma and paranglioma. *Ann Surg Oncol* 2020;27:1329-37.
4. Woolen S, Gemmete JJ. Parangliomas of the head and neck. *Neuroimaging Clin N Am* 2016;26:259- 78.
5. Gilbo P, Morris CG, Amdur RJ, et al. Radiotherapy for benign head and neck parangliomas: a 45-year experience. *Cancer* 2014;120:3738-43.
6. Hu K, Persky MS. Treatment of head and neck parangliomas. *Cancer Control* 2016;23:228-41.
7. Mukherji SK, Kasper ME, Tart RP, Mancuso AA. Irradiated parangliomas of the head and neck: CT and MR appearance. *AJNR Am J Neuroradiol* 1994;15:357-63.

8. Kim S, Loevner L, Quon H, et al. Diffusion-weighted magnetic resonance imaging for predicting and detecting early response to chemoradiation therapy of squamous cell carcinomas of the head and neck. *Clin Cancer Res* 2009;15:986-94.
9. Fangberget A, Nilsen LB, Hole KH, et al. Neoadjuvant chemotherapy in breast cancer-response evaluation and prediction of response to treatment using dynamic contrast-enhanced and diffusion-weighted MR imaging. *Eur Radiol* 2011;21:1188-99.
10. Gaeta M, Benedetto C, Minutoli F, et al. Use of diffusion-weighted, intravoxel incoherent motion, and dynamic contrast-enhanced MR imaging in the assessment of response to radiotherapy of lytic bone metastases from breast cancer. *Acad Radiol* 2014:1286-93.
11. Thoeny HC, De Keyzer F, King AD. Diffusion-weighted MR imaging in the head and neck. *Radiology* 2012;263:19- 32.
12. Srinivasan A, Dvorak R, Perni K, Rohrer S, Mukherji SK. Differentiation of benign and malignant pathology in the head and neck using 3T apparent diffusion coefficient values: early experience. *AJNR Am J Neuroradiol* 2008;29:40- 4.
13. Koontz NA, Wiggins RH 3rd. Differentiation of benign and malignant head and neck lesions with diffusion tensor imaging and DWI. *AJR Am J Roentgenol* 2017;208:1110- 5.
14. Zhao M, Guo LL, Huang N, et al. Quantitative analysis of permeability for glioma grading using dynamic contrast-enhanced magnetic resonance imaging. *Oncol Lett* 2017;14:5418-26.



15. Roberts HC, Roberts TP, Brasch RC, Dillon WP. Quantitative measurement of microvascular permeability in human brain tumors achieved using dynamic contrast-enhanced MR imaging: correlation with histologic grade. *AJNR Am J Neuroradiol* 2000;21:891-9.
16. Tischler AS, deKrijger RR. 15 years of paraganglioma: pathology of pheochromocytoma and paraganglioma. *Endocr Relat Cancer* 2015;22:123-33.
17. Offergeld C, Brase C, Yaremchuk S, et al. Head and neck paragangliomas: clinical and molecular genetic classification. *Clinics (Sao Paulo)* 2012;67 Suppl 1(Suppl 1):19- 28.
18. Ahlawat S, Khandheria P, Grande FD, et al. Interobserver variability of selective region-of-interest measurement protocols for quantitative diffusion weighted imaging in soft tissue masses: comparison with whole tumor volume measurements. *J Magn Reson Imaging* 2016;43:446-54.
19. Han X, Suo S, Sun Y, et al. Apparent diffusion coefficient measurement in glioma: influence of region-of-interest determination methods on apparent diffusion coefficient values, interobserver variability, time efficiency, and diagnostic ability. *J Magn Reson Imaging* 2017;45:722-30.
20. Jansen JC, van den Berg R, Kuiper A, van der Mey AG, Zwinderman AH, Cornelisse CJ. Estimation of growth rate in patients with head and neck paragangliomas influences the treatment proposal. *Cancer* 2000;88:2811-6.
21. Wang JT, Wang AY, Cheng S, Gomes L, Da Cruz M. Growth rate analysis of an untreated glomus vagale on MRI. *Case Rep Otolaryngol* 2016;2016:8756940.

22. Heesterman BL, de Pont LMH, Verbist BM, et al. Age and tumor volume predict growth of carotid and vagal body paragangliomas. *J Neurol Surg B Skull Base* 2017;78:497-505.
23. Chang CA, Pattison DA, Tothill RW, et al. (68) Ga-DOTATATE and (18)F-FDG PET/CT in paraganglioma and pheochromocytoma: utility, patterns and heterogeneity. *Cancer Imaging* 2016;16:22.
24. Telischi FF, Bustillo A, Whiteman ML, et al. Octreotide scintigraphy for the detection of paragangliomas. *Otolaryngol Head Neck Surg* 2000;122:358- 62.

Author Manuscript

## Tables

Table 1. Patients' demographics

Patient	Sex	Age	Location	RT	Pre-treatment volume (cm <sup>3</sup> )	Post-treatment volume (cm <sup>3</sup> )	Pre ADC/Post ADC ( $\times 10^{-3}$ mm <sup>2</sup> /s)	Pre nADC/Post nADC	Pre Ve/Post Ve	Pre Kep/Post Kep	Pre Vp/Post Vp	Pre Ktrans/Post Ktrans
1	M	36	L jugular fossa	EBRT,45Gy/25Fr	7.07	4.88	1.38/1.53	1.84/2.04	0.67/0.42	1.65/0.91	0.16/0.33	1.44/0.31
2	F	66	L jugular fossa	EBRT,50Gy/25Fr	4.85	4.03	1.35/1.53	1.80/2.04	0.57/0.21	6.78/4.21	0.30/0.30	1.68/0.95
3	M	46	L jugular fossa	SRT,25Gy/5Fr	7.53	5.57	1.13/1.53	1.51/2.05	0.35/0.48	2.17/0.66	0.48/0.48	0.69/0.30
4	F	59	L jugular fossa	EBRT,50.4Gy/28Fr	1.98	1.58	0.88/1.05	1.17/1.40	0.15/0.10	1.71/1.66	0.44/0.48	0.31/0.10
5	F	53	R jugular fossa	EBRT,45Gy/25Fr	3.43	3.43	1.17/1.34	1.56/1.79	0.46/0.64	15.63/4.79	0.32/0.32	2.15/1.94

6	F	61	R jugular fossa	EBRT,50Gy/25F r	28.1	21.5	1.36/1.6 8	1.81/2. 24	0.24/0. 20	3.58/1.1 3	0.31/0. 41	1.05/0.3 4
7	F	54	L jugular fossa	EBRT,50Gy/25F r	89.5	72.5	1.05/1.2 5	1.40/1. 67	0.59/0. 35	5.49/1.5 0	0.31/0. 31	1.46/0.3 8
8	F	42	R carotid bifurcati on	EBRT,50Gy/25F r	10.4	4.89	0.59/1.1 7	0.79/1. 56	0.23/0. 19	0.52/1.7 3	0.42/0. 42	0.52/0.3 8
9	F	58	L jugular fossa	SRT,30Gy/5Fr	2.66	2.66	1.36/1.1 2	1.81/1. 49	0.54/0. 20	3.53/0.9 5	0.31/0. 36	1.44/0.1 7
10	F	63	R carotid bifurcati on	SRT,30Gy/5Fr	12.31	8.12	0.91/1.3 7	1.21/1. 83	0.76/0. 43	2.58/0.8 1	0.15/0. 15	1.46/0.2 7
11	F	69	R jugular fossa	EBRT,45Gy/25F r	2.13	3.26	1.20/1.3 5	1.60/1. 80	0.24/0. 37	8.39/7.4 4	0.34/0. 36	2.33/2/ 94

M = male, F = female, R = right, L = left, RT = radiation therapy, EBRT = external beam radiation therapy, SRT = stereotactic radiotherapy, Gy = gray, Fr = fractions, ADC = apparent diffusion coefficient, Vp = blood plasma volume per unit tissue volume, Ve = extravascular, extracellular space (EES) volume per unit tissue volume, Kep = rate transfer constant between EES and blood plasma per minute, Ktrans = volume transfer constant between EES and blood plasma per minute

Table 2. ADC values and quantitative parameters between pre- and post-treatment status

	Pre-treatment status	Post-treatment status	P-value
Mean ADC value ( $\times 10^{-3}$ mm <sup>2</sup> /s)	1.25 $\pm$ 0.25	1.36 $\pm$ 0.20	.005
Normalized mean ADC value	1.50 $\pm$ 0.33	1.81 $\pm$ 0.26	.005
V <sub>p</sub>	0.32 $\pm$ 0.10	0.36 $\pm$ 0.09	.07
V <sub>e</sub>	0.44 $\pm$ 0.21	0.33 $\pm$ 0.16	.10
K <sub>ep</sub> (minute <sup>-1</sup> )	4.82 $\pm$ 4.31	2.34 $\pm$ 2.18	.027
K <sub>trans</sub> (minute <sup>-1</sup> )	1.32 $\pm$ 0.64	0.73 $\pm$ 0.89	.007

Values are described as mean  $\pm$  standard deviation. ADC = apparent diffusion coefficient, V<sub>p</sub> = blood plasma volume per unit tissue volume, V<sub>e</sub> = extravascular, extracellular space (EES) volume per unit tissue volume, K<sub>ep</sub> = rate transfer constant between EES and blood plasma per minute, K<sub>trans</sub> = volume transfer constant between EES and blood plasma per minute

Table 3. Relationship of ratio of volume (post-treatment status/pre-treatment status) and pretreatment parameters.

	Mean ADC value	Normalized mean ADC value	Vp	Ve	Kep	Ktrans
Correlation coefficient (r)	0.42, 95% CI(0.25-0.81)	0.42, 95% CI(0.25-0.81)	0.036, 95% CI(-0.58-0.62)	-0.19, 95% CI(-0.71-0.46)	0.59, 95% CI(0.02-0.88)	0.70, 95% CI(0.18-0.92)
P-value	.20	.20	.92	.58	.058	.016

CI= Confidence intervals, ADC = apparent diffusion coefficient, Vp = blood plasma volume per unit tissue volume, Ve = extravascular, extracellular space (EES) volume per unit tissue volume, Kep = rate transfer constant between EES and blood plasma per minute, Ktrans = volume transfer constant between EES and blood plasma per minute

Table 4. Relationship of ratio of volume (post-treatment status/pre-treatment status) and posttreatment parameters.

	Mean ADC value	Normalized mean ADC value	Vp	Ve	Kep	Ktrans
Correlation coefficient (r)	-0.06, 95% CI(-0.64-0.56)	-0.06, 95% CI(-0.64-0.56)	-0.017, 95% CI(-0.61-0.59)	0.19, 95% CI(-0.46-0.71)	0.8, 95% CI(0.37-0.94)	0.83, 95% CI(0.45-0.95)
P-value	.87	.86	.96	.58	.003	.002

CI= Confidence intervals, ADC = apparent diffusion coefficient, Vp = blood plasma volume per unit tissue volume, Ve = extravascular, extracellular space (EES) volume per unit tissue volume, Kep = rate transfer constant between EES and blood plasma per minute, Ktrans = volume transfer constant between EES and blood plasma per minute

Figure 1 A 61-year-old male with paraganglioma in the right jugular foramen. (a) Post-contrast T1 weighted image, (b) apparent diffusion coefficient (ADC) map, and (c) permeability map demonstrate a pre-treatment paraganglioma in the right jugular foramen. (d) Post-contrast T1-weighted image, (e) ADC map, and (f) permeability map demonstrate a post-treatment paraganglioma. A freehand region of interest (ROI) is placed on (b) and (e) ADC maps, and pre-and post-treatment ADC values are calculated. Another freehand ROI is placed on (c) and (f) permeability maps, and quantitative parameters are calculated. In this case, the tumor regresses after external beam radiation therapy.

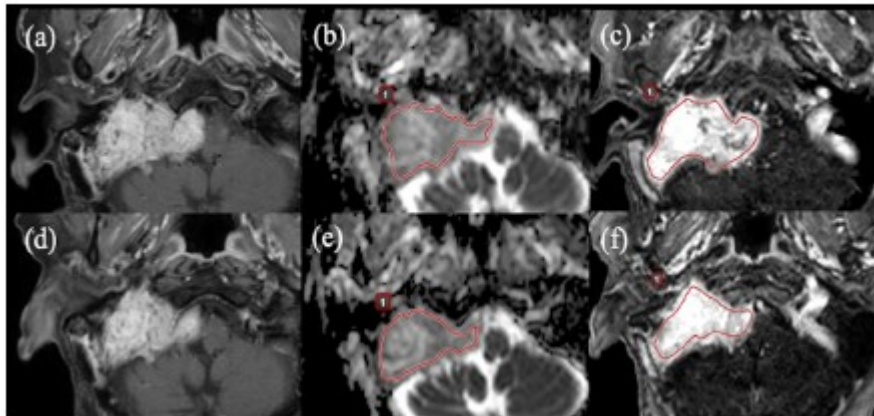


Figure 2 A 69-year-old female with paraganglioma in the right jugular foramen. (a) Post-contrast T1 weighted image, (b) apparent diffusion coefficient (ADC) map, and (c) permeability map demonstrate a pretreatment paraganglioma in the right jugular foramen. (d) Post-contrast T1-weighted image, (e) ADC map, and (f) permeability map demonstrate a post-treatment paraganglioma. A freehand region of interest (ROI) is placed on (b) and (e) ADC maps, and pre-and post-treatment ADC values are calculated. Another freehand ROI is placed on (c) and (f) permeability maps, and quantitative parameters are calculated. In this case, the tumor grows after external beam radiation therapy. In addition, the tumor invades the right mastoid air cells and results in opacification.

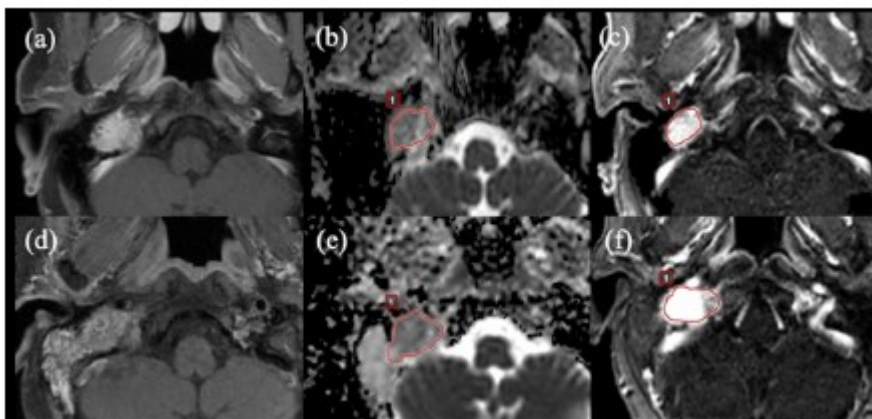
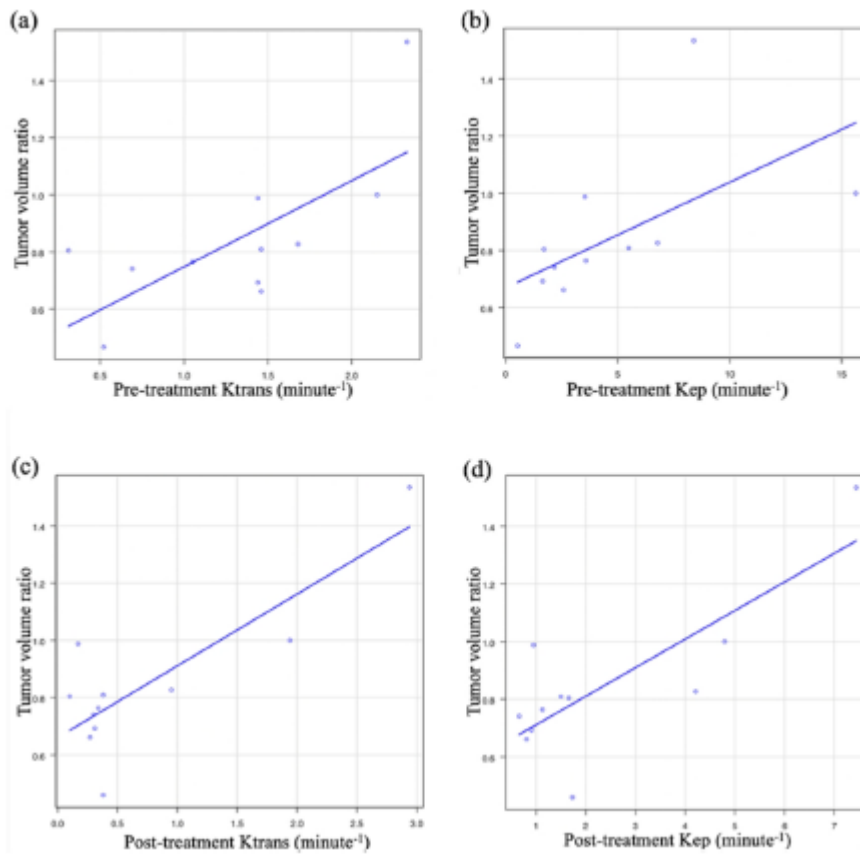




Figure 3 (a) and (b) show the regression lines of the relationship between tumor volume ratio (posttreatment status/pre-treatment status) and pre-treatment Ktrans (volume transfer constant between extravascular, extracellular space (EES) and blood plasma per minute) and Kep (rate transfer constant between EES and blood plasma per minute) ( $r = 0.70$ ;  $P = .016$ ,  $r = 0.59$ ;  $P = .058$ , respectively). (c) and (d) show the regression lines of the relationship between tumor volume ratio and post-treatment Ktrans and Kep ( $r=0.83$ ;  $P = .002$ ,  $r=0.8$ ;  $P=.003$ , respectively).



Autho